JOURNAL OF PROPULSION AND POWER
Vol. 16, No. 5, September–October 2000

Propagation of Spinning Acoustic Modes in Turbofan Exhaust Ducts

M. Nallasamy*
DYNACS Engineering Company, Brook Park, Ohio 44142
D. L. Sutliff†
AYT Corporation, Cleveland, Ohio 44135
and
L. J. Heidelberg‡
NASA John H. Glenn Research Center at Lewis Field, Cleveland, Ohio 44135

A theoretical and experimental study of sound propagation in a turbofan exhaust duct is presented. The effect of duct-area change on the propagation of rotor-stator interaction tones is studied. The pressure reflection coefficient and far-field directivity shape variations as a result of duct termination, duct-flow Mach number, and exhaust hub-to-tip radius ratio are examined. A finite element method and a modal analysis technique that is employed in induct mode measurements are used. The computational results show that even with large changes in duct area there is no transfer of modal power from one mode to another, as it propagates through varying cross-sectional area. However, as the exhaust hub-to-tip radius ratio increases, higher-order radial modes get cut off. Exponential horn termination keeps the principal lobe peak angle fixed for the first-order radial modes at the design speed. Increases in flow Mach number and exhaust hub-to-tip radius ratio move the principal lobe peak angle away from the exhaust duct axis. This reduces the axial beaming of acoustic energy of low-order spinning modes and enhances absorption by acoustic liners. The computed axial variation of acoustic power in the duct and phase angle of acoustic pressure show good agreement with the experimental data.

Introduction

IN modern high-bypass-ratioturbofan engines fan noise is a critical component controlling the total noise at takeoff and approach conditions. A better understanding of the fan noise generation, propagation, and radiation will aid in the design of noise suppression devices to alleviate community noise problems. A typical fan noise spectrum consists of tone noise [blade passing frequency (BPF) and its harmonics] superimposed over broadband noise. The fan tone noise is the result of interactions of periodic disturbances of the rotor-blade mean wakes with the stator vanes. This is usually referred to as rotor-stator interaction noise, and it is the component considered here.

The fan noise generated has a spinning mode structure while propagating within the inlet or exhaust ducts. Knowledge of the modal structure is useful in predicting the propagation in the duct and the radiation directivity pattern. The spinning mode analysis of the fan noise was first introduced by Tyler and Sofrin.[1] In any plane normal to a cylindrical annular fan duct axis, the periodic acoustic pressure may be represented as the real part of

$$p(\theta, r, t) = \sum_{m=-\infty}^{\infty} \sum_{n=0}^{\infty} C_{mn}[J_m(k_{mn}r) + Q_{mn}Y_m(k_{mn}r)]e^{i(m\theta - \omega t)} \tag{1}$$

Here m specifies the circumferential mode number, and n indicates the associated radial mode number. J_m and Y_m are the Bessel functions of the first and second kind, respectively; k_{mn} is the transverse eigenvalue of the (m, n) mode; and k_{mn} and Q_{mn} are functions of fan hub-to-tip radius ratio σ. θ is the circumferential (angular) coordinate, and ω is the frequency. C_{mn} is the modal amplitude, and r is the radius normalized by the duct radius R:

$$Q_{mn} = -J'_m(\sigma k_{mn}) / Y'_m(\sigma k_{mn})$$

For a given frequency ω and circumferential mode order m, the radial distribution of acoustic pressure in the annular duct reduces to

$$p(r) = \sum_{n=0}^{\infty} C_{mn}[J_m(k_{mn}r) + Q_{mn}Y_m(k_{mn}r)] \tag{2}$$

The acoustic pressure is the physical quantity that can be measured for comparison between theory and experiment. A spinning mode of order m and frequency ω will propagate through the duct only if the cutoff ratio ξ is greater than or equal to unity. The cutoff ratio is defined as

$$\xi = \frac{(\omega/c)R}{k_{mn}\sqrt{1 - M^2}} \tag{3}$$

where M is the nominal duct flow Mach number and c is the speed of sound.

The noise generated at the stator propagates upstream through the rotor and inlet duct and downstream through the stator and exhaust duct. The fan inlet and exhaust ducts usually vary in cross-section area along the duct axis. The effect of moderate area change of the inlet ducts on sound propagation was the subject of several investigations (see, for example, Refs. 2–5). The area change of the fan exhaust ducts along the axis is sometimes more severe than considered in those studies. In this paper the effects of duct-area change on the propagation of spinning acoustic modes in fan exhaust ducts and radiation to the far field are investigated using the finite element technique developed by Eversman.[6] A modal analysis technique that is used to study induct modal structure is employed to extract the modal content from the finite element solution. This is

Presented as Paper 99-0481 at the AIAA 37th Aerospace Sciences Meeting, Reno, NV, 11–14 January 1999; received 29 January 1999; revision received 8 July 1999; accepted for publication 10 July 1999.

*Supervisor. Senior Member AIAA.
†Research Engineer. Senior Member AIAA.
‡Aerospace Engineer. Senior Member AIAA.

done to examine the effect of duct-area change on the modal structure. The effects of duct termination and duct-flow Mach number on the pressure reflection coefficient and far-field directivity are also studied.

The axial variation of acoustic pressure in the duct with area change is experimentally measured for different cutoff ratios of the mode (2, 0) at BPF. The computed duct power and phase angle of acoustic pressure are compared with the experimental data.

Propagation in the Exhaust Duct and Radiation

The sound propagation in the duct and the radiation from the duct termination to the far field are studied using the Eversman code.[6] The code is based on a frequency-domain, finite element, formulation of acoustic propagation. It solves the acoustic field (both inside and outside of the duct) once the internal geometry of the duct and the in-duct pressure level are specified. The specification of the internal acoustic field is in terms of the amplitudes of the cut-on modes [Eq. (2)] at the internal boundary (source plane) of the computational domain. The computational domain is the region that starts at the input plane inside the duct—source plane, stator leading edge—and extends outside of the duct between the duct axis and a suitably chosen baffle (Fig. 1). Care is taken to keep the baffle position far away from the source region so that its effect on the solution is negligible. On the far-field boundary and on the baffle, a Sommerfield radiation condition is specified.

Because the dynamics of the exhaust jet shear layer is highly complicated, a simplified model is used. The shear layer is modeled as though the duct extends some distance downstream of the exit plane. In the extended region the flow is composed of two parts, an inner flow and an outer flow, and the velocity potential is discontinuous across the layer separating them. But, beyond the extended region the velocity potential is assumed to be continuous and the internal and external flows are allowed to mix on a potential flow basis. The extent of the fictitious duct is chosen as to provide realistic acoustic-wave diffraction effects across the shear layer while at the same time minimizing the influence of artificial mixing on the acoustic field. This treatment of the shear layer is found to work reasonably well for the moderate-flow Mach numbers considered here. For the acoustic calculations the presence of the shear layer necessitates the specification of two continuity conditions along the interface. These are the continuity of acoustic pressure across the shear layer and the continuity of displacement of the interface itself. The latter is a kinematic condition arising from the assumption that the interface acts as an impermeable membrane across which acoustic perturbations are transmitted by virtue of its motion.

The geometry and the mean flow are assumed to be axially symmetric, and the mean flow is taken to be inviscid and irrotational. The acoustic field equations are obtained by considering small perturbations superimposed on the mean flow. The noise source is decomposed into its circumferential modal content, allowing for a two-dimensional representation of the acoustic field in an (x, r) plane through the axis of symmetry.

The sound field at the source plane (Fig. 1), stator leading edge, is specified in terms of duct mode amplitudes of radial orders in a single circumferential mode. The acoustic potential field is expressed as a combination of the incident and reflected (positive and negative) uniform duct eigenfunctions. The acoustic potential ϕ is written as

$$\phi = \sum_{n=0}^{N} \phi_n^+ e^{-k_{x_n}^+ x} e_n(r) + \sum_{n=0}^{N} \phi_n^- e^{-k_{x_n}^- x} e_n(r) \tag{4}$$

Here ϕ_n^+ and ϕ_n^- are the incident and reflected duct mode amplitudes, $k_{xn}^{\pm}$ are the axial wave numbers, N is the number of (radial) modes retained in the expansion, and $e_n(r)$ is the duct eigenfunction corresponding to each retained duct mode. When the input is given in terms of specified value of incident (ϕ^+) modal amplitude, the reflected mode (ϕ^-) amplitude is obtained as a part of the solution. The reflection is caused by the duct termination.

The potential mode amplitudes are related to the acoustic pressure amplitudes by

$$p_n^{\pm} = -i\rho_0 \eta_r \left[1 - U_f \left(k_{x_n}^{\pm} / \eta_r\right)\right] \phi_n^{\pm} \tag{5}$$

where ρ_0 is the mean flowfield density, $\eta_r = (\omega R/c)$ is the reduced frequency, and U_f is the mass-averaged axial velocity at the source plane. The reflection coefficient is computed as the magnitude of the ratio of reflected/incident acoustic pressure amplitudes (p^-/p^+).

The Eversman finite element code was used recently to study the noise radiation from the NASA Glenn Active Noise Control Fan (ANCF) geometry[7] and to make data-theory comparisons of a model high-speed fan configuration.[8] In both cases the code was found to model the spinning acoustic mode propagation in the duct and radiation to the far field reasonably accurately.

Duct Modal Analysis

The finite element solution gives the acoustic pressure distribution in the duct. At any axial station (with or without area change), from the radial distribution of acoustic pressure the radial mode content can be obtained in the same way as it is extracted from the measured radial distribution of pressure from[9]

$$p_{m,r} = \sum_{n=0}^{\infty} P_{m,n} E_{mn}(k_{mn} r) \tag{6}$$

where E_{mn} is the radial mode function given by

$$E_{mn} = A_{mn} \Psi_{mn} \tag{7}$$

$$\Psi_{mn}(k_{mn} r) = [J_m(k_{mn} r) + Q_{mn} Y_m(k_{mn} r)] \tag{8}$$

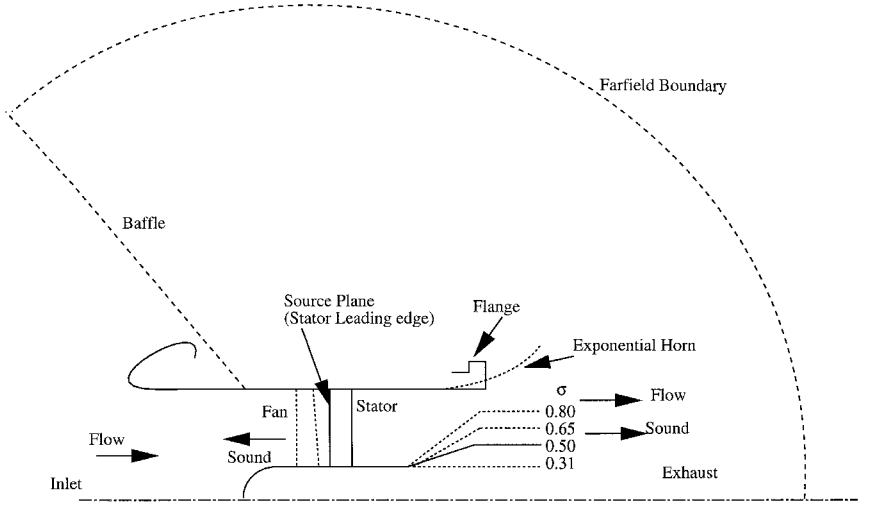

Fig. 1 Sketch of the computational domain.

$P_{m,n}$ is the modal pressure coefficient of mode (m, n), and $p_{m,r}$ is the physical pressure of the circumferential mode order m at a given frequency. J_m, Y_m, and Q_{mn} are the same as defined in Eq. (1).

A_{mn} is a normalizing constant, which ensures that the integral of power squared across the duct is unity. This means that the square of the coefficient of a mode term of the form of Eq. (1) represents the power in that mode. A_{mn} is given by

$$1/A_{mn}^2 = \pi\left[\left(1 - m^2/k_{mn}^2\right)\Psi_{mn}^2(k_{mn}) - \left(\sigma^2 - m^2/k_{mn}^2\right)\Psi_{mn}^2(k_{mn}\sigma)\right] \quad (9)$$

In the preceding expression σ is the hub-to-tip radius ratio. A finite number of radial modes N_m is assumed to exist, and the modal pressure coefficient $P_{m,n}$ is obtained by a least-squares curve fit by minimizing total mean square error defined as

$$\text{error}^2 = \sum_{i=1}^{N_p}\left[\sum_{n=0}^{N_m} P_{m,n}E_{mn}(k_{mn}r) - p_{m,r}\right]^2 \quad (10)$$

where N_p is the number of radial points at which pressure is input for this analysis. $N_p = 20$ is used in the present study. The radial mode amplitude, phase angle, cutoff ratio, and mode power are computed at each desired axial station. The expression for power P appropriate for a uniform moving medium is given by

$$P = \int_{A_d}\left[(1 + M^2)\langle pu_x^*\rangle + M\left(\langle pp^*\rangle/\rho c + \rho c\langle u_x u_x^*\rangle\right)\right] \quad (11)$$

where u_x is the axial component of the acoustic particle velocity, p is the acoustic pressure, A_d is the cross-sectional area of the duct, and ρ is the medium nominal density. Superscript $*$ denotes the complex conjugate. The symbol $\langle\cdot\rangle$ denotes time averaging over one period, $2\pi/\omega$.

The present study was done using the basic geometry of the ANCF that is used for aeroacoustic research at NASA John H. Glenn Research Center at Lewis Field.[7,10] The ANCF test bed and the experimental setup for the present investigation are described next.

ANCF Test Bed

The ANCF[10] uses a 16-bladed variable-pitch rotor and can be configured with stator vanes to provide specific mode generation and propagation for aeroacoustic research. A unique feature on the ANCF is the direct attachment of the rotor centerbody to the rig support column, eliminating the need for struts, which could contaminate acoustic measurements. Additionally, an Inflow Control Device (ICD) allows for static testing. The combination of low tip speed (~400 ft/s [122 m/s]) and the 48-in. (121.9-cm) diam produces fan tones of the same frequencies produced by full-size advanced engines. The nozzle-area contraction is accomplished by an increase in the centerbody diameter to get the desired hub-to-tip radius ratio at the exit. A schematic of the ANCF is shown in Fig. 2a.

The primary measurement device on the ANCF is the rotating rake.[9] The rotating rake is an implementation of a technique originally conceived by T. G. Sofrin,[11] whereby a rake containing radially distributed pressure transducers rotates in the circumferential direction at a precise fraction of the fan rotational speed. Because each circumferential acoustic mode is known to rotate at a unique speed[1] in the rotor reference frame, a Doppler shift is induced in the rake reference frame. Further reduction of the data into radial modes is accomplished through a least-squares curve fit to Bessel basis functions.

The ANCF is located in the NASA John H. Glenn Research Center's Aeroacoustic Propulsion Laboratory (APL), a hemispherical anechoic (to 125 Hz) test facility. Far-field measurements are taken from 28 microphones at 50 ft (15.24 m) in the ANCF horizontal plane. The SPL data from these microphones are corrected to 40 ft (12.19 m), standard day conditions.

Experimental Setup

The ANCF was configured with 14 stator vanes located $\frac{1}{2}$ chord spacing for the present experiment (Fig. 2a). The exhaust duct was modified to be able to test two exit hub-to-tip radius ratios, $\sigma = 0.5$ and 0.65. The modifications included a removable extended centerbody (Fig. 2b) and an additional 13-in. (33-cm) duct spool piece for duct extension. The baseline configuration had a constant-area annular duct (of fan hub-to-tip radius ratio $\sigma = 0.307$), followed by a converging section, and followed by another constant-area section to the exit plane. The hub-to-tip radius ratio at the exit plane is 0.50 for this configuration. The extended centerbody configuration extended the converging section all the way to the exit plane such that the exit plane hub-to-tip radius ratio was 0.65.

Rotating-rake data were obtained at two axial locations (Fig. 2a) in the exhaust duct for each configuration. Position #1 was located just before the ramp section. Position # 2 was located just after the end of the ramp section, for the nominal configuration ($\sigma = 0.5$). This corresponded to approximately a midconverging section for the extended centerbody configuration ($\sigma = 0.65$). Also, data were taken with a static axial rake installed at the exit plane.

An array of microphones was used to verify the Eversman code duct propagation computations. Sixteen hearing-aid type microphones were installed on a single axial line on the outer wall of the exhaust duct. This line of microphones was at a constant circumferential angle, i.e., bottom dead center. Table 1 and Fig. 2a show the axial locations of these microphones. The time histories of each microphone signal were synchronously acquired using the fan shaft encoder (128 samples per revolution). A time history length of 1250 fan revolutions was acquired and time domain-averaged (TDA) with an ensemble length of one revolution. An FFT 128 point was performed on the TDA signal to obtain magnitude and phase of the wall pressure at BPF.

The ANCF is known to generate rotor-stator interaction modes at least 15 dB above extraneous modes. Hence, the assumption was made that the entire signal measured by the axial array microphones was caused by the primary interaction mode or (2, 0) at BPF. This may cause a slight error. At the locations where wall microphones exist near the rotating-rake position, the difference is within interpolation error. At the microphones located in the forward part of the array, which are actually in the plane of the stator vanes, the expectation is that the influence of decaying modes may be significant.

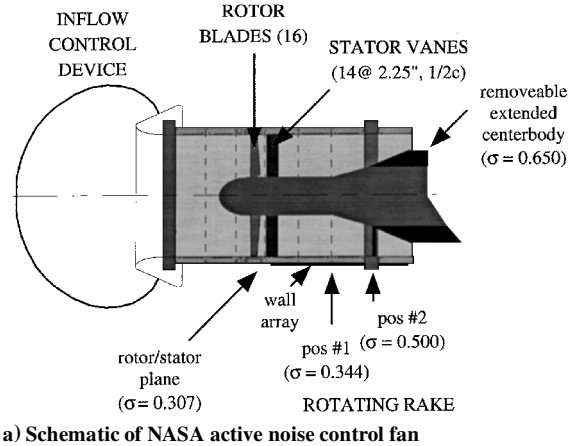

a) Schematic of NASA active noise control fan

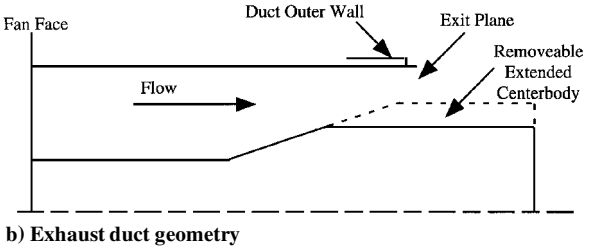

b) Exhaust duct geometry

Fig. 2 Experimental arrangement.

Table 1 Axial microphone array and other critical axial locations

Mic #	Loc, in. (cm)
Stator l.e.	1.875 (4.76)
1	3.000 (7.62)
2	6.250 (15.88)
Stator t.e	6.375 (16.19)
3	9.500 (24.13)
4	12.750 (32.39)
5	14.625 (37.15)
6	18.375 (46.67)
7	22.125 (56.20)
8	25.875 (65.72)
Rake pos #1	29.625 (75.25)
Ramp begins	31.500 (80.01)
9	33.250 (84.46)
10	36.500 (92.71)
11	39.750 (100.97)
Rake pos #2	42.625 (108.27)
12	43.000 (109.22)
13	46.250 (117.48)
Ramp ends (nom.)	46.500 (118.11)
14	49.500 (125.73)
15	52.750 (133.98)
Ramp ends (ext.)	55.625 (141.29)
16	56.000 (142.24)
Exit plane	58.625 (148.91)

The pressure measured at the wall was further modified to account for the area change effects along the duct. This was done so that the change in pressure magnitude along the wall array caused by reflections could be analyzed independently of the change in area. The formula was similar to the calculations used for power. This may be termed apparent power because it would be the power if no reflection existed. The power reported as measured by the rotating rake is computed in a similar way, without discriminating the forward going and reflected components. The primary component is assumed to be the forward going wave generated by the rotor-stator interaction. If the reflection is significantly strong, the power calculated will be in error.

Results and Discussion

Theoretical Results

In the present study the basic geometry of ANC fan was used (Fig. 1). The fan stage has 16 rotor blades and 14 stator vanes. At the design speed of 1880 rpm, the following modes (m, n) propagate: BPF: (2, 0); 2BPF: (4, 0), (4, 1); 3BPF: (6, 0), (6, 1), (6, 2). The propagation of these modes through the duct with varying area of cross section was studied. A unit amplitude input is specified at the source plane. For this study the source plane is moved 1 duct radius upstream to provide sufficient duct length to study propagating modes at low cutoff ratios. The effects of duct-flow Mach number, exhaust hub-to-tip radius ratio, and duct termination on the pressure reflection coefficient, principal lobe angle, and far-field levels are described. The far-field levels were computed at the far-field boundary located at 20 duct radii. Comparisons with the experimental data are presented and discussed in the Experimental Results section.

Modal Structure and Mode Power

To study the effect of duct-area change on the acoustic power distribution in the radial mode orders, the flanged termination is replaced by an exponential horn termination (Fig. 1). This avoids the complications associated with changes in mode reflection coefficient, with exhaust hub-to-tip radius ratio, that may affect modal power. Three exhaust hub-to-tip radius ratios, 0.50, 0.65, and 0.80, were considered to examine the effect of area change. For comparison, an annular duct with fan hub-to-tip radius ratio of 0.307 with no exhaust area change was also considered (Fig. 1). The duct acoustic pressure distribution for each hub-to-tip radius ratio is obtained with unit modal input at the source plane. From the pressure distribution the modal characteristics along the duct can be examined in detail

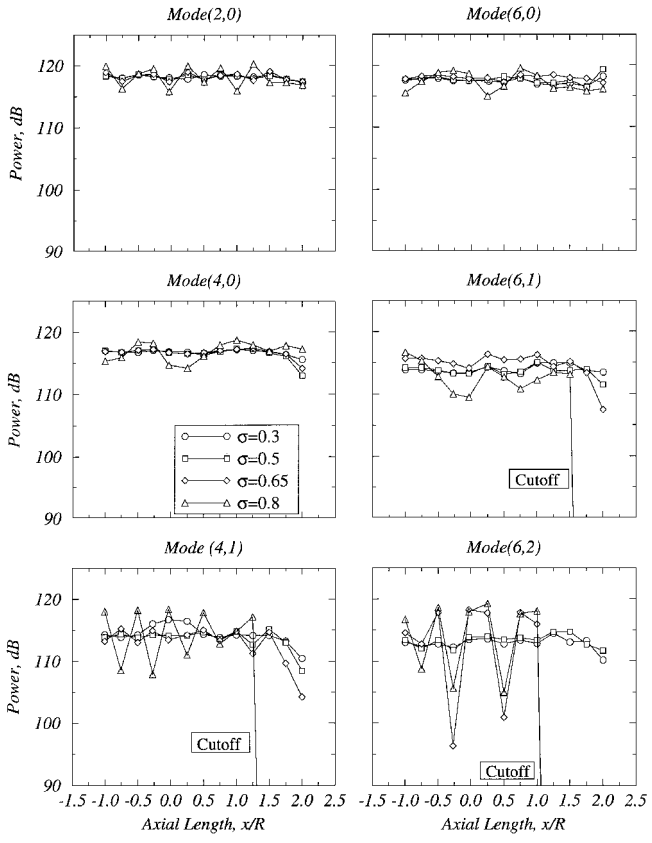

Fig. 3 Effect of duct-area change on duct modal power: 1880 rpm and $M = 0.1$.

as explained in the modal analysis section. Modal characteristics examined are the phase angle of acoustic pressure and power variations for each mode along the duct. The specific question of modal power variation in each harmonic tone is summarized in Fig. 3 for the first three harmonics. For BPF tone the extracted modal characteristics from radial pressure variation along the changing area duct do not show any variation in mode power with an exhaust hub-to-tip radius ratio of as high as 0.80. In the case of 2BPF, the first radial (4, 0) is unaffected going through the area change while mode (4, 1) gets cutoff at an axial distance of 1.25, consistent with the hub-to-tip radius ratio at that location. However, no discernible transfer of power from one radial order to another occurs because of reduction in area. A similar behavior is observed at 3BPF. The power level of (6, 0) mode is unaffected by the duct-area change, from a hub-to-tip radius ratio of 0.3–0.8. Mode (6, 1) is cutoff at the axial station 1.5 for a hub-to-tip radius ratio of 0.8, and the (6, 2) mode is cutoff at $x/R = 1.0$ for hub-to-tip ratios 0.65 and 0.80. That is, with increase in exhaust hub-to-tip radius ratio, higher radial order modes get cutoff as they go through a reduction in area of exhaust duct. However, there is no indication of acoustic power transfer from one radial to the other because of area change.

Pressure Reflection Coefficient

The basic ANCF configuration with a flange termination is used for the results reported in this and the sections that follow. The variations of the pressure reflection coefficient with cutoff ratio ξ and reduced frequency η_r are shown in Fig. 4. First-order radials have the highest reflection coefficients, and they increase with decrease in cutoff ratio (left column of Fig. 4). The higher-order radials (4, 1), (6, 1), and (6, 2) also show increase of reflection coefficient with reduction in cutoff ratio. For mode (6, 1) the increase is not monotonic, and this appears to be because scattering into neighboring modes is dominant at certain cutoff ratios for this mode. The variation of reflection coefficient with reduced frequency is shown in the right column of Fig. 4. The results confirm the belief that the reflection is generally insignificant, except for the modes near cutoff ratio of unity.

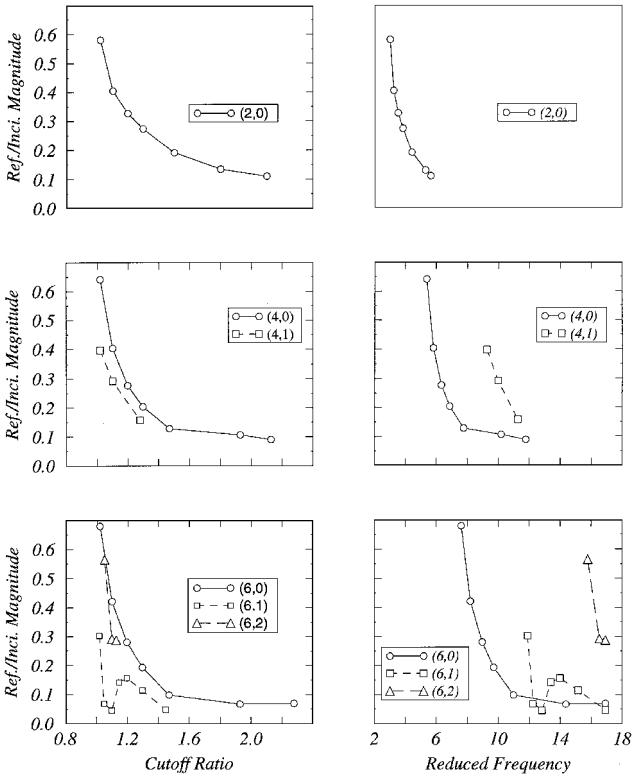

Fig. 4 Variation of pressure reflection coefficient with cutoff ratio and reduced frequency, $\sigma = 0.5$. Modes: BPF = (2, 0); 2BPF = (4, 0), (4, 1); and 3BPF = (6, 0), (6, 1), and (6, 2).

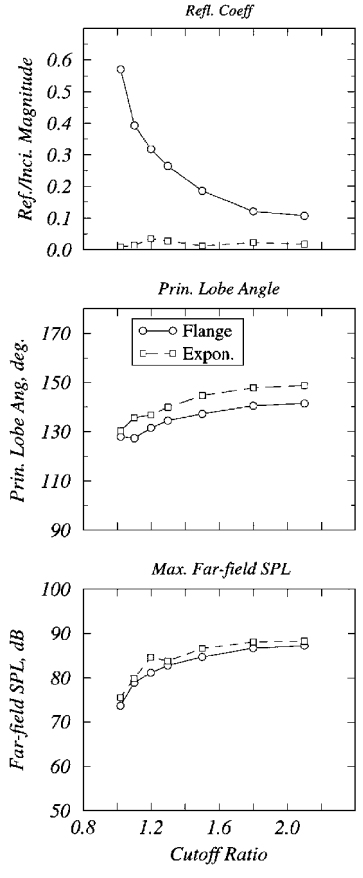

Fig. 5 Influence of duct termination on the pressure reflection coefficient, principal lobe angle, and maximum far-field sound pressure level: $\sigma = 0.5$ and mode (2, 0).

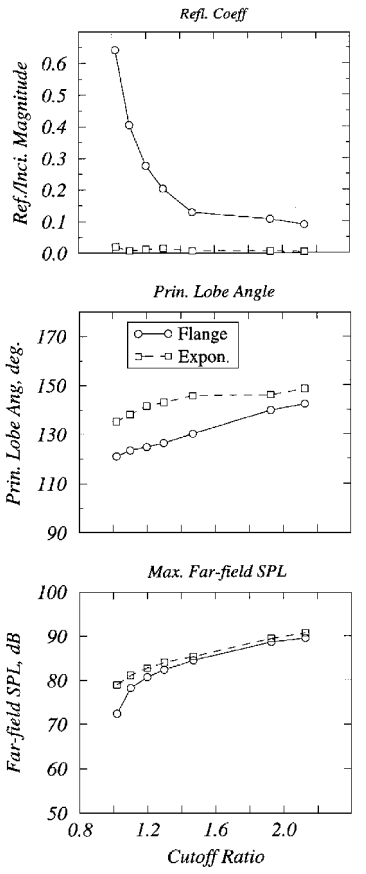

Fig. 6 Influence of duct termination on the pressure reflection coefficient, principal lobe angle, and maximum far-field sound pressure level: $\sigma = 0.5$ and mode (4, 0).

Duct Termination

The mode reflection coefficient, principal lobe peak angle, and the maximum far-field sound pressure level (SPL) are compared for ANCF-flanged duct termination and exponential horn termination in Figs. 5–7. The results for mode (2, 0) are shown in Fig. 5. With exponential termination the reflection coefficient is negligible at all cutoff ratios as would be expected. The principal lobe peak angle moves toward the exhaust duct axis (The far-field angle shown is with respect to inlet axis. Angle 180 deg refers to exhaust duct axis.) compared to the flanged termination. The maximum far-field SPL is consistently higher for exponential termination, and the maximum difference of 3 dB occurs at a cutoff ratio of 1.2. The behavior of mode (4, 0) is shown in Fig. 6. The difference in far-field SPL increases with reduction in cutoff ratio. For this mode the movement of the principal lobe angle towards the exhaust duct axis is also significant. Figure 7 shows the reflection coefficient and far-field shapes for mode (6, 0). The characteristics are similar to that of (4, 0) mode. The far-field directivity shapes for the three modes are shown in Fig. 8. The observation is made that at the design speed the peak principal lobe moves toward the exhaust duct axis for the exponential horn termination. The principal lobe angle is about 150 deg and is the same for all three modes, (2, 0), (4, 0), and (6, 0), with exponential horn termination in contrast to the flanged termination.

Duct-Flow Effects

The effect of duct-flow Mach number on the reflection coefficient and far-field shapes are shown in Fig. 9. The reflection coefficient decreases with increase in duct Mach number from 0.1 to 0.25 at all cutoff ratios for modes (2, 0), (4, 0), and (6, 0). Such reduction in reflection coefficient with flow was also observed in inlet duct propagation studies.[4] The principal lobe angle moves away from the exhaust duct axis at all cutoff ratios, as the Mach number is

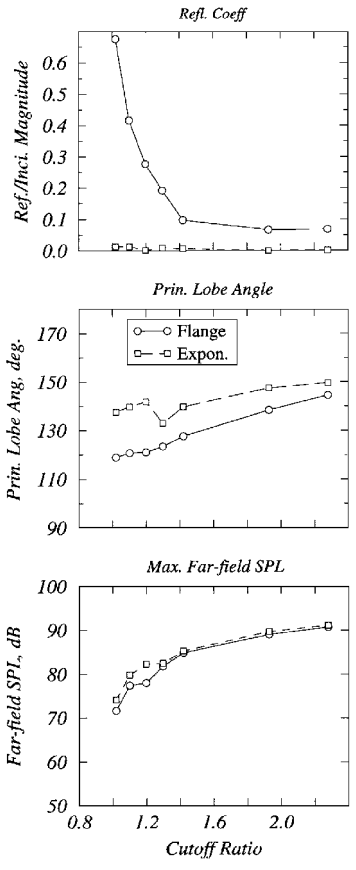

Fig. 7 Influence of duct termination on the pressure reflection coefficient, principal lobe angle, and maximum far-field sound pressure level: σ = 0.5 and mode (6, 0).

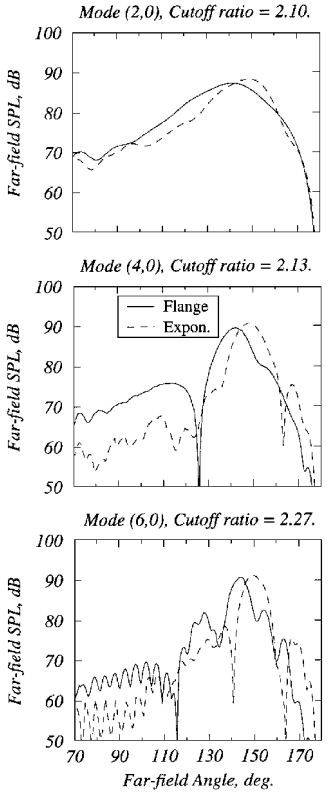

Fig. 8 Influence of duct termination on far-field directivity: σ = 0.5 and 1880 rpm.

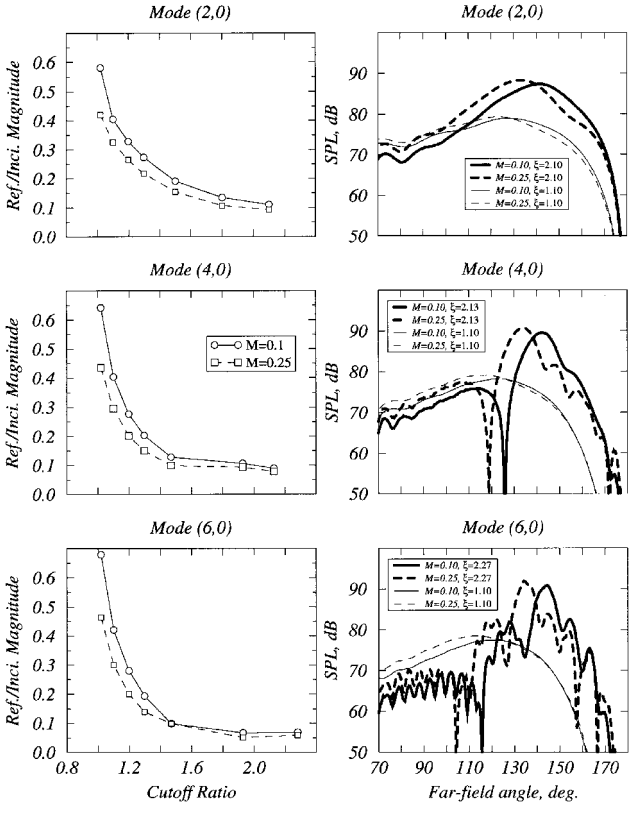

Fig. 9 Effect of duct-flow Mach number on the pressure reflection coefficient and far-field directivity. σ = 0.5, flange termination.

increased. This effect is consistent with that reported by Nallasamy.[7] As stated in that reference, and also, observed in inlet duct studies,[4] the principal lobe angle of the inlet radiation is insensitive to the duct-flow Mach number.

Effect of Exhaust Hub-to-Tip Radius Ratio

The effects of hub-to-tip radius ratio of the exhaust on the reflection coefficient and far-field directivity are shown in Fig. 10. The increase in hub-to-tip radius ratio from 0.5 to 0.65 increases the reflection coefficient at all of the reduced frequencies except for $\eta_r = 3.2$ and 3.01 where the reflection coefficient is lower than that for $\sigma = 0.5$. For the mode (4, 0) a somewhat different behavior is observed. The reflection coefficient for this mode shows little change with increased hub-to-tip radius ratio except for reduced frequencies 5.81 and 5.39, where the reflection coefficient for $\sigma = 0.65$ is lower than that for $\sigma = 0.5$. The reflection coefficients for mode (6, 0) is, in general, lower for $\sigma = 0.65$ than that for $\sigma = 0.5$. The right column of Fig. 10 shows the directivity shapes for the three modes. The principal lobe peak angle moves away from the exhaust duct axis for all modes and the far-field shapes vary significantly with hub-to-tip radius ratio.

Experimental Results

The mode (2, 0) profile along the duct wall measured by the wall array was compared to that computed by the Eversman finite element code. Experimentally, the basis for comparison was the apparent power calculated from the wall microphones. Computationally, the mode (2, 0) power was computed using the complete radial profile at each axial station.

Figure 11 compares the experimentally measured apparent power to the computed acoustic power for the nominal configuration ($\sigma_{ex} = 0.50$). Mode (2, 0) axial profiles are shown for 3 corrected fan rpm, 1000, 1400, and 1800. These speeds correspond to mode (2, 0) cutoff ratios of 1.02, 1.43, and 1.83, respectively. Comparisons of magnitude and phase are shown. Mode (2, 0) data from the rotating rake are also plotted. Because of the finite element solution

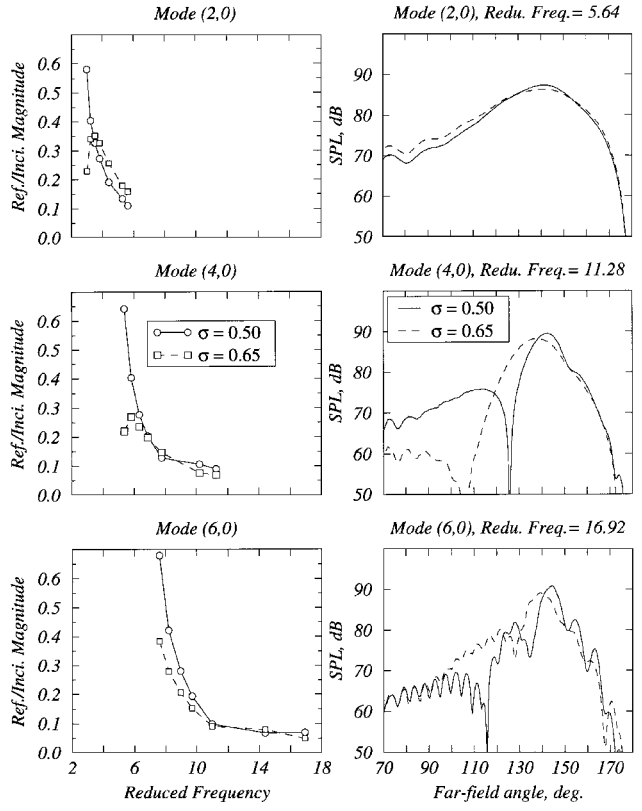

Fig. 10 Influence of hub-to-tip radius ratio on the pressure reflection coefficient and far-field directivity: mode (2, 0), mode (4, 0), and mode (6, 0).

with unit amplitude input, the computed power at the axial station corresponding to the rotating-rake location is matched to the power measured by the rotating rake. The phase angle from the code was adjusted to match at the exit plane. Table 1 is useful to compare axial locations with the data stations.

The acoustic power of the (2, 0) mode is shown on the left side of Fig. 11, and the phase of the acoustic pressure is shown on the right side. In general, the computed variation along the duct axis agrees well with the data.

The data at 1800 rpm, where the (2, 0) mode is well cut on, agrees very well. The axial wavelength is approximately 0.6 times the duct length. A slight interference pattern is noted with minimums at 14, 35, and 46 in. (35.56, 88.90, and 116.84 cm). The variation in phase shows the expected cycle and the agreement between code and data are excellent. In all cases the microphone data near the origin is suspect. The first two microphone locations are between the leading and trailing edge of the stators and are definitely subject to errors such as being in the potential field.

At 1400 rpm the axial wavelength is approximately equal to the duct length, and a sharp interference at 43 in. (109.22 cm) is noted in the experimental data. The code accurately predicts the location of this interference. The predicted power level is, however, higher than that measured. The rotating-rake measured power level also shows a milder cancellation, probably because of the point resolution of wall microphone seeing a stronger local interference. The code also predicts another interference at 15 in. (38.10 cm). This may be seen in the data at this location, but at this location the assumption that the wall mics are measuring only (2, 0) is less accurate. The phase variation at 1400 rpm shows nearly one complete cycle as would be expected based on the axial wavelength being nearly equal to the duct length.

The comparisons between the computed and experimental results at 1000 rpm show a more qualified agreement. At distances greater than 40 in. (101.60 cm), the agreement in magnitude is excellent. At locations closer to the source plane, a significant error is noted. This is most obvious in the phase profile. The axial wavelength

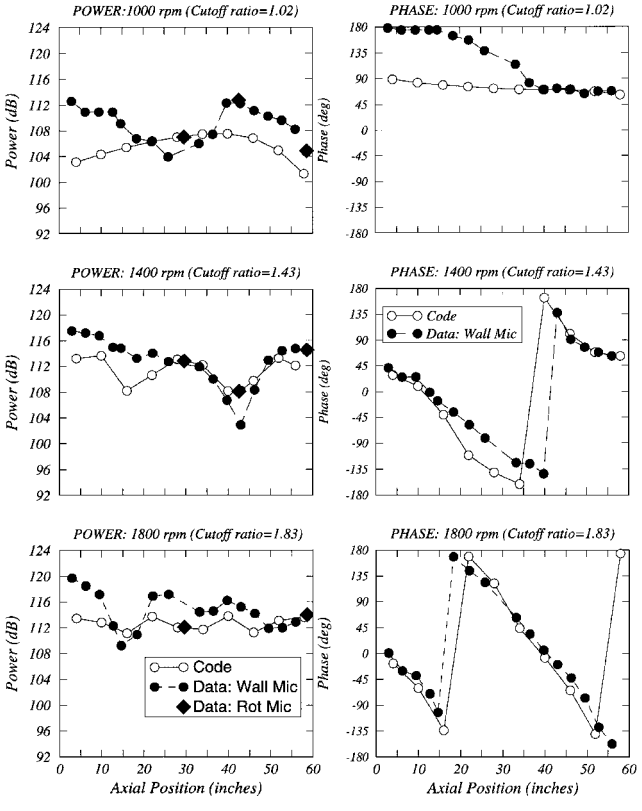

Fig. 11 Measured and computed axial variation of acoustic power and phase angle of acoustic pressure at 1000, 1400, and 1800 rpm: σ = 0.5 and mode (2, 0).

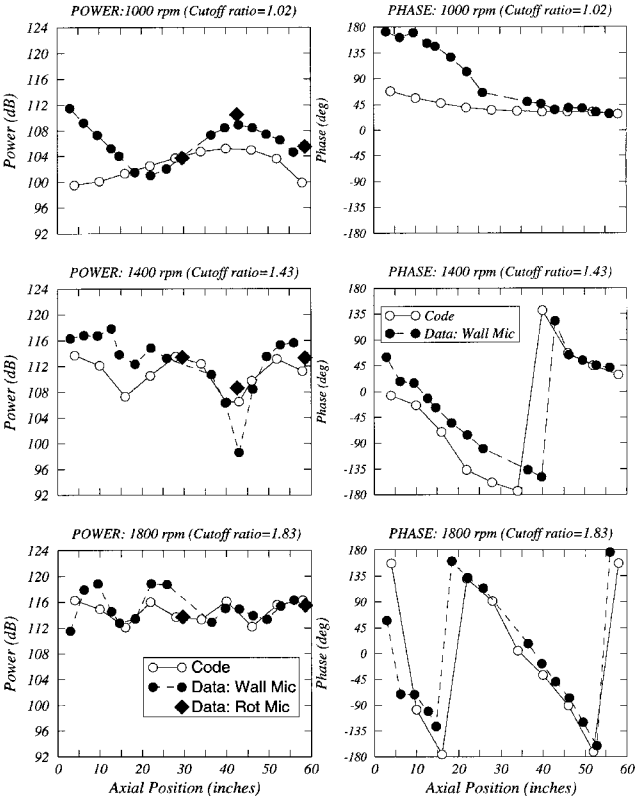

Fig. 12 Measured and computed axial variation of acoustic power and phase angle of acoustic pressure at 1000, 1400, and 1800 rpm: σ = 0.65 and mode (2, 0).

at 1000 rpm is several times the duct length. Also, near cutoff the variation in axial wavelength is much more sensitive to the change in cutoff ratio caused by area change. At the rotor-stator plane the axial wavelength is about 7.3 times the duct length; at the exit 1.7 times. At these ratios the expectation is that the phase variation would be small, and this is demonstrated by the code. The data, however, show a phase shift of approximately 90 deg between the source region and the region further downstream in the duct. Is this phase shift similar to the phase shift that one observes between the near field and far field of a dipole source in free field? It is not clear. The complexity increases because the mode is very near cutoff. Further study is needed to clarify this. The microphones in the source region are being strongly influenced by the potential field of the stators. This is also seen in the higher magnitude levels near the source.

Figure 12 shows the axial power variation for the extended centerbody configuration ($\sigma = 0.65$) at the same cutoff ratios as already stated, which are defined at the rotor-stator plane. A comparison of Figs. 11 and 12 shows minimal difference in the profiles at corresponding speeds. This indicates the length of the ramp, or converging section, has minimal impact.

Conclusions

Sound propagation in exhaust ducts of varying cross section has been examined. Even with very large area changes, there is no transfer of modal power from one mode to another. Reflection has negligible effect except for modes near cutoff. An increase in exhaust hub-to-tip ratio produces a mode-dependent variation in pressure reflection coefficient and far-field shape. The principal lobe peak angle moves away from exhaust duct axis with increase in flow Mach number at all cutoff ratios, consistent with earlier findings. The computed axial variations of acoustic power and phase angle of acoustic pressure from the finite element solution show good agreement with the experimental data.

References

[1]Tyler, J. M., and Sofrin, T. G., "Axial Flow Compressor Noise," *SAE Transactions*, Vol. 70, 1962, pp. 309–332.

[2]Tam, C. K. W., "Transmission of Spinning Acoustic Modes in a Slightly Non-Uniform Duct," *Journal of Sound and Vibration*, Vol. 18, No. 3, 1971, pp. 339–351.

[3]Cho, Y. C., and Ingard, K. U., "Closed-Form Solution of Mode Propagation in a Non-Uniform Circular Duct," *AIAA Journal*, Vol. 20, No. 1, 1982, pp. 39–44.

[4]Silcox, R. J., and Lester, H. C., "Sound Propagation Through a Variable Area Duct: Experiment and Theory," *AIAA Journal*, Vol. 20, No. 10, 1982, pp. 1377–1384.

[5]Nayfeh, A. H., Shaker, B. S., and Kaiser, J. E., "Transmission of Sound Through Circular Ducts with Compressible Mean Flows," *AIAA Journal*, Vol. 18, No. 5, 1980, pp. 515–525.

[6]Eversman, W., "Aft Fan Duct Acoustic Radiation," CEAS/AIAA Paper 95-155, June 1995.

[7]Nallasamy, M., "Computation of Noise Radiation from Fan Inlet and Aft Ducts," *Journal of Aircraft*, Vol. 34, No. 3, 1997, pp. 387–393.

[8]Envia, E., and Nallasamy, M., "Design Selection and Analysis of a Swept and Leaned Stator Concept," NASA TM-208662, Dec. 1998.

[9]Hall, D. G., Heidelberg, L. J., and Konno, K., "Acoustic Mode Measurements in the Inlet of a Model Turbofan Using a Continuously Rotating Rake: Data Collection and Analysis Techniques," AIAA Paper 93-0599, Jan. 1993.

[10]Heidelberg, L. J., Hall, D. G., Bridges, J. E., and Nallasamy, M., "A Unique Ducted Fan Test Bed for Active Noise Control and Aeroacoustic Research," AIAA Paper 96-1740, May 1966.

[11]Cicon, D. E., Sofrin, T. G., and Mathews, D. C., "Investigation of Continuously Traversing Microphone System for Mode Measurement," NASA CR-168040, Nov. 1982.